Tuning the magnetostructural phase transition in FeRh nanocomposites

Radhika Barua, Xiujuan Jiang, Felix Jimenez-Villacorta, J. E. Shield, D. Heiman, and L. H. Lewis

Citation: Journal of Applied Physics **113**, 023910 (2013); doi: 10.1063/1.4774282
View online: https://doi.org/10.1063/1.4774282
View Table of Contents: http://aip.scitation.org/toc/jap/113/2
Published by the American Institute of Physics

Tuning the magnetostructural phase transition in FeRh nanocomposites

Radhika Barua,[1] Xiujuan Jiang,[2] Felix Jimenez-Villacorta,[1] J. E. Shield,[2] D. Heiman,[3] and L. H. Lewis[1]
[1]*Department of Chemical Engineering, Northeastern University, Boston, Massachusetts 02115, USA*
[2]*Department of Mechanical Engineering, University of Nebraska, Lincoln, Nebraska 68588, USA*
[3]*Department of Physics, Northeastern University, Boston, Massachusetts 02115, USA*

(Received 30 August 2012; accepted 18 December 2012; published online 11 January 2013)

Effects of nanostructuring on the magnetostructural response of the near-equiatomic FeRh phase were investigated in nanocomposite materials synthesized by rapid solidification and subsequent annealing of an alloy of nominal atomic composition $(FeRh)_5Cu_{95}$. Transmission electron microscopy studies confirm attainment of a phase-separated system of nanoscaled (~10–15 nm diameter) precipitates, consistent with FeRh embedded in a Cu matrix. These nanoprecipitates are crystallographically aligned with the coarse-grained Cu matrix and possess an $L1_0$-type (CuAu 1) structure, in contrast to the B2 (CsCl)-type structure of bulk FeRh. It is proposed that the face-centered cubic crystal structure of the Cu matrix serves as a template for the formation and stabilization of the $L1_0$ structure in the FeRh nanoprecipitates. Magnetic measurements highlight the existence of multiple magnetic phases in the material exhibiting spin-glass ($T \leq 15$ K), ferromagnetic and paramagnetic ($T > 20$ K) behavior. A thermally hysteretic magnetic transition, remarkably similar to the magnetostructural transition of bulk CsCl-type FeRh reported at $T_t = 370$ K, is observed in the nanostructured material at 130 K. This result not only emphasizes the sensitivity of the magnetic and structural properties of FeRh to changes in microstructural scale, but also highlights the potential for tailoring magnetostructural transitions in functional materials systems via nanostructuring. © *2013 American Institute of Physics*. [http://dx.doi.org/10.1063/1.4774282]

I. INTRODUCTION

Magnetostructural phase transitions are of considerable interest to the research community in both basic and applied scientific areas due to the recognition that selected materials in the vicinity of these transitions have the capability of providing exceptionally large functional effects in response to small excursions in magnetic field, temperature, and strain.[1–3] These transitions comprise simultaneous magnetic and structural phase changes of an abrupt and hysteretic nature, emphasizing strong coupling between the spins, orbitals, and lattice of a given system. Magnetostructural transitions are thermodynamically first-order and thus produce a discontinuity in the first derivatives of the Gibbs free energy $G(T,P)$, where T is the temperature and P is the pressure of the system. It is envisioned that magnetostructural materials may have significant potential for technological, environmental, and economic impact as they can be incorporated into a wide array of magnetic devices ranging from actuators[4] to networked environmental sensors for energy harvesting[3] and for energy management.[5,6]

Based on theoretical predictions,[7,8] it is recognized that in addition to modification of extrinsic variables—temperature (T), pressure (P), and magnetic field (H)—reduction of the characteristic dimensions of the system via nanostructuring may also provide an alternative route for engineering magnetostructural phase transitions in functional materials systems. In this work, FeRh serves as a test bed to explore the effects of nanostructuring on the magnetostructural response. In its bulk form, the near-equiatomic phase of $Fe_{1-x}Rh_x$ ($0.47 \leq x \leq 0.53$) has a cubic B2 ((CsCl)-type) crystal structure that exhibits an abrupt antiferromagnetic (AFM) to ferromagnetic (FM) transition with heating to $T \sim 350$ K,[9] accompanied by a unit cell volume increase of 1%.[10] Giant magnetoresistance,[11] giant magetocaloric,[12] and giant volume magnetostriction[13] effects have been reported in this compound, with the magnetostructural transition driven by a multitude of physical inputs such as pressure,[12–16] magnetic field,[16,17] and temperature.[18] Further, the FeRh magnetostructural transition temperature is reported to be sensitive to addition of transition-metal and noble metal impurities.[17,19–21]

Although extensive research has been carried out on bulk and thin film forms of FeRh,[9–23] limited work has been performed on nanoscaled FeRh systems.[24–26] Previous reports indicate that chemically synthesized FeRh nanoparticles of controlled composition and size (4–20 nm, Ref. 26) undergo a hysteretic magnetic transition at around T_t ($H = 1$ T) ~ 320 K; this transformation is very broad, a feature that may be attributed either to reduced particle size or to surface oxidation effects. Furthermore, it is noted that attainment of the ordered CsCl phase in the chemically synthesized FeRh nanoparticles is inconclusive. To date, the relationship between the structural and magnetic properties of FeRh systems with nanoscale dimensions remains unclear.

In the current work, effects of nanostructuring on the magnetostructural transition of near-equiatomic $Fe_{1-x}Rh_x$ alloys are examined through the synthesis of a rapidly solidified alloy of composition $(FeRh)_5Cu_{95}$. Since the elements Fe and Rh have very limited solid solubility in Cu,[27,28] it was hypothesized that non-equilibrium synthesis of $(FeRh)_5Cu_{95}$ ribbons would yield non-interacting nanoscaled

FeRh precipitates in a Cu matrix upon moderate annealing. Indeed, as shall be demonstrated, characterization of rapidly solidified and annealed ribbons of this study confirms attainment of nanoprecipitates (~10–15 nm diameter) that are crystallographically coherent with the coarse-grained Cu matrix. Significantly, these nanoprecipitates exhibit a $L1_0$ (CuAu 1)-type structure, instead of the anticipated B2 (CsCl)-type structure found in bulk FeRh. A thermally hysteretic magnetic transition, remarkably similar to the magneto-structural transition of bulk CsCl-type FeRh reported at $T_t = 370$ K, is observed in the nanostructured material at 130 K. Broadly speaking, these results highlight the potential for tailoring magnetostructural transitions by nanostructuring.

II. EXPERIMENTAL DETAILS

A phase-separated system of coherent nanoscaled FeRh precipitates (~10–15 nm diameter) embedded in a Cu matrix was synthesized via rapid solidification and subsequent annealing of a pre-alloyed, arc-melted charge of nominal atomic composition $(FeRh)_5Cu_{95}$ (99.99% purity). Rapid solidification was carried out by melt-spinning in an Ar atmosphere with a tangential quenching wheel speed of 31 m/s. The resultant ribbons were ~3 mm wide and ~100 μm thick, with lengths >2 cm and highly reflective surfaces. Isochronal annealing for 30 min was carried out in a tube furnace in the temperature range $100\,^{\circ}C \leq T \leq 800\,^{\circ}C$ at intervals of 100 °C. To avoid oxidation during annealing at high temperatures as well as to foster consistent magnetic measurements, 20–40 mg samples were sealed and measured in vitreous silica tubes (3 mm o.d., 1.8 mm i.d.) in a nominal vacuum of 1×10^{-6} Torr.[29] For comparison purposes and to facilitate identification of the magnetic phases in the $(FeRh)_5Cu_{95}$ nanocomposite, control samples consisting of melt-quenched ribbons of Cu containing dilute amounts of Fe or Rh were also synthesized, annealed, and measured under the same conditions. The nominal compositions of the control samples were $Cu_{98}Fe_2$ and $Cu_{98}Rh_2$.

Correlations between the crystallographic character and the magnetic response of these metallic ribbons were studied using several structural and magnetic probes. Scanning electron microscopy energy-dispersive X-ray spectroscopy (SEM-EDS) was used to confirm the chemical composition and homogeneity of the rapidly solidified ribbons in their as-quenched state. The structural properties of the as-quenched and annealed ribbons were examined with standard laboratory Cu Kα X-ray diffraction (XRD) and transmission electron microscopy (TEM—JEOL 2010 TEM operating at 200 kV). TEM sample preparation was accomplished by mechanically polishing the melt-spun ribbons to a thickness of ~10 μm, followed by ion milling to perforation using a Gatan Precision Ion Polishing System (PIPS) operated at 5 kV. A least-squares fit was applied to the XRD data to estimate lattice parameters.[30] The magnetic behavior of the system was investigated by superconducting quantum interference device (SQUID) magnetometry in fields up to $H = 5$ T and temperatures in the range $2\,K \leq T \leq 400\,K$ in both zero-field-cooled (ZFC) and field-cooled (FC) conditions.

III. RESULTS

A. Structural attributes

The chemical homogeneity and composition of rapidly solidified $(FeRh)_5Cu_{95}$, $Cu_{98}Fe_2$, and $Cu_{98}Rh_2$ ribbons were confirmed using SEM-EDS. In all samples, no crystalline phases other than face-centered cubic (fcc) Cu with a slightly expanded lattice parameter, $a = 3.620 \pm 0.001$ Å (relative to the standard Cu lattice parameter of $a = 3.615$ Å (Ref. 31)) was observed using laboratory XRD. However, TEM studies indicated that the microstructure of the annealed $(FeRh)_5Cu_{95}$ ribbons consists of micron-scale polycrystalline grains containing nanoscale (~10 nm) precipitates, shown in Fig. 1(a). TEM selected-area electron diffraction (SAED) patterns taken along the $[1\bar{1}0]$ zone axis show the presence of Bragg reflections arising from both the matrix and the precipitates, shown in Fig. 1(b). The TEM SAED pattern of the matrix indexes to a fcc structure consistent with the XRD data. Intriguingly, instead of the expected B2 (CsCl)-type structure found in bulk FeRh, diffraction information obtained from the nanoprecipitates is consistent with the $L1_0$ (CuAu 1)-type crystal structure with lattice parameters $a = 4.32$ Å and $c = 4.20$ Å. The lattice parameters of the $L1_0$-ordered precipitates are estimated to have accuracy of 2%–3%,[32] resulting in an estimated error on the order of 0.13 Å. The $L1_0$-ordered structure in the precipitates was determined through the appearance of superlattice reflections in the SAED pattern. In Figure 1(b), the $L1_0$-reflections corresponding to the precipitate phase are clearly marked. Expectedly, the intensity of the super lattice reflection from the {110} plane of the $L1_0$-ordered FeRh phase is weak.[32] A definite orientational relationship is observed between the Cu matrix and the precipitate phase: $<110>_{Cu}//<110>_{FeRh}$ for directions and $\{001\}_{Cu}//\{001\}_{FeRh}$ for planes. It is to be

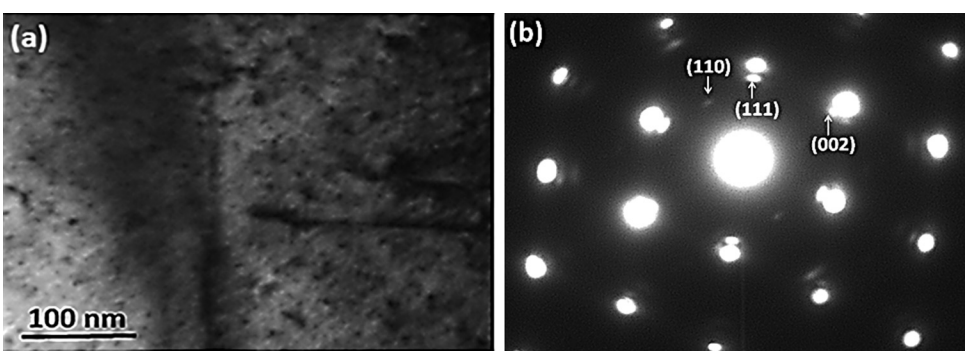

FIG. 1. (a) Plan-view TEM images of annealed $(FeRh)_5Cu_{95}$ ribbons showing the presence of nanoprecipitates with ~10–15 nm diameters in micron-scaled grains of Cu. (b) TEM diffraction pattern of annealed $(FeRh)_5Cu_{95}$ ribbons showing that the precipitates have an orientational relationship with the Cu matrix. Arrows indicate the crystallographic orientation corresponding to the precipitate reflections.

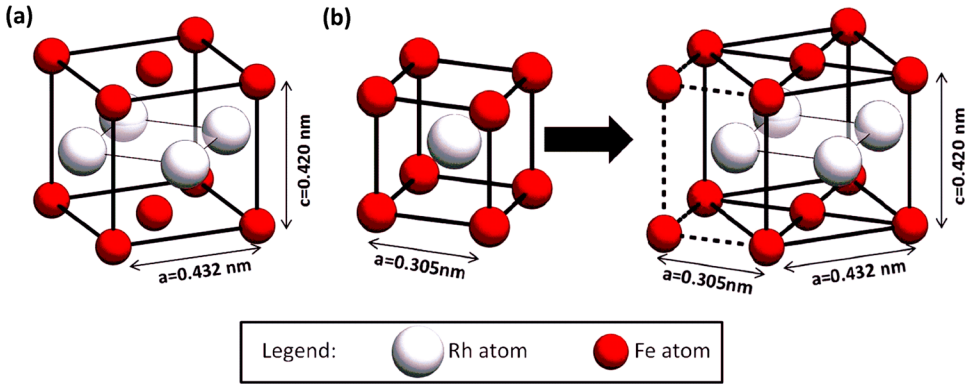

FIG. 2. (a) Schematic illustration of the $L1_0$-type ordered crystal structure of the FeRh nanoprecipitates. (b) Schematic illustration of the relationship between the B2 and $L1_0$ crystal phases of FeRh (also known as Bain correspondence).

noted that the $L1_0$ (CuAu 1) crystal structure is an ordered crystallographic derivative of the face-centered tetragonal (fct) crystal structure, where four of the tetragonal unit cell faces are occupied by one type of atom and the corner and the other faces are occupied with the second type of atom. The relationship between the B2 and $L1_0$ crystal structures—also known as a Bain correspondence[33]—is shown schematically in Fig. 2.

B. Magnetic attributes

Temperature- and field-dependant magnetization of rapidly solidified ribbons of composition $(FeRh)_5Cu_{95}$, $Cu_{98}Fe_2$, and $Cu_{98}Rh_2$ was studied in fields up to 5 T and temperatures in the range $2\,K \leq T \leq 400\,K$. The magnetic behavior of the $(FeRh)_5Cu_{95}$ nanocomposite system is described first, followed by a brief discussion of the magnetic behavior of $Cu_{98}Fe_2$ and $Cu_{98}Rh_2$ ribbons.

The magnetic behavior of the $(FeRh)_5Cu_{95}$ ribbons is categorized into three temperature regimes: (1) low temperature ($2\,K \leq T \leq 15\,K$); (2) intermediate temperature ($15\,K \leq T \leq 200\,K$); and (3) high temperature ($T \geq 200\,K$). In the low-temperature regime ($2\,K \leq T \leq 15\,K$), the $(FeRh)_5Cu_{95}$ ribbons show spin-glass-like behavior. Fig. 3 displays the low-temperature ZFC susceptibility curves of the ribbons in as-quenched and annealed states. The blocking temperature (T_b) of the spin-glass phase in the as-quenched $(FeRh)_5Cu_{95}$ ribbons, defined as the peak of the dc susceptibility curves $\chi(T)$, is $T_b = 10\,K$. Annealing the ribbons to 500 °C reduces T_b to 6.5 K.

In Fig. 4, the ZFC and FC temperature-dependent magnetization curves of as-quenched and annealed $(FeRh)_5Cu_{95}$ ribbons in the intermediate temperature range ($15\,K \leq T \leq 200\,K$) are shown. In the as-quenched state, the ribbons demonstrate paramagnetic behavior. Following Bitter *et al.*,[40] the overall paramagnetic susceptibility (χ_{tot}) can be described by the sum of Curie-Weiss-type susceptibility (first term) and temperature-independent Pauli paramagnetic susceptibility (second term)

$$\chi_{\text{tot}} = \frac{C}{T-\theta} + \chi_{\text{pp}}, \tag{1}$$

where C is the Curie constant, θ is the paramagnetic Curie temperature, and χ_{pp} is the temperature independent Pauli paramagnetic susceptibility. A fit to the data obtained from the as-spun material using Eq. (1) provided the following parameters: $C = 1.98 \times 10^{-3}$ cm^3/g of $Cu_{95}(FeRh)_5$; $\theta = 0.69\,K$; $\chi_{pp} = 1.93 \times 10^{-5}$ cm^3/g of $Cu_{95}(FeRh)_5$.

After annealing the ribbons to $T > 200\,°C$, a magnetic transition is observed with an onset at $T_t = 130\,K$. In Fig. 5(a),

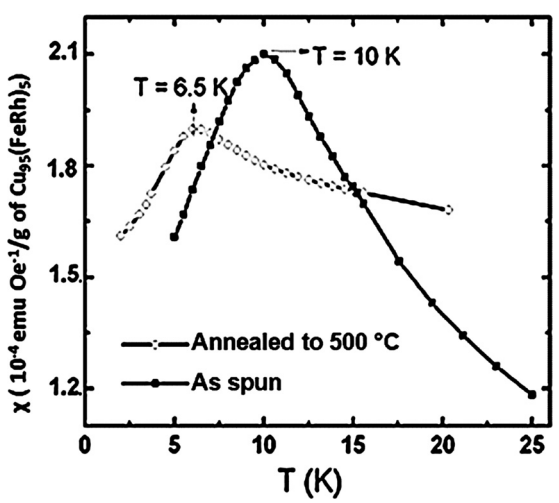

FIG. 3. Low-temperature zero-field-cooled susceptibility of $(FeRh)_5Cu_{95}$ ribbons showing evidence of a spin-glass phase. The blocking temperature (T_b) of the spin-glass phase is defined at the peak of the susceptibility curves $\chi(T)$. Annealing decreases T_b.

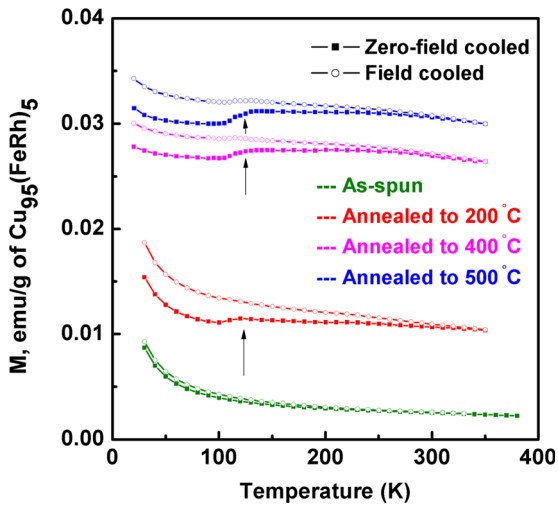

FIG. 4. ZFC and FC temperature-dependant magnetization curves of $(FeRh)_5Cu_{95}$ ribbons in as-quenched as well as annealed conditions ($H = 100$ Oe). Arrows indicate the presence of the secondary phase with a magnetic transition at $T \sim 130\,K$ which forms upon annealing.

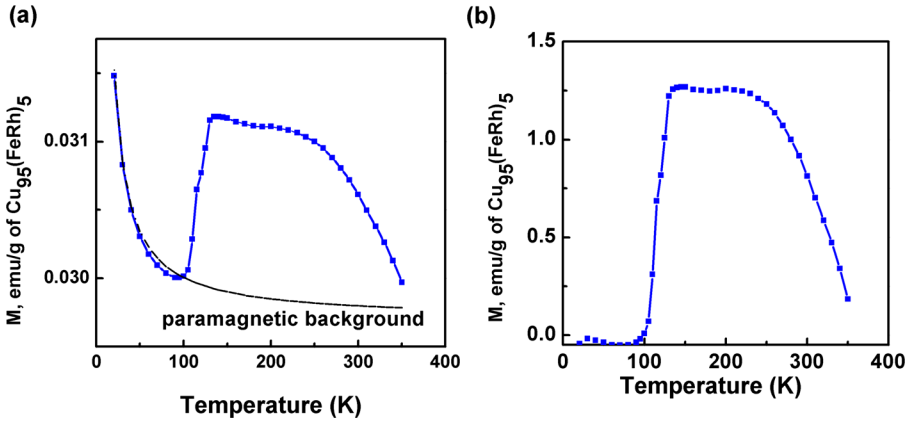

FIG. 5. (a) An expanded view of the zero-field-cooled temperature-dependent magnetization curve for $(FeRh)_5Cu_{95}$ ribbons annealed to 500 °C. (b) Temperature dependence of the magnetic moment of the annealed $(FeRh)_5Cu_{95}$ ribbons after subtraction of the paramagnetic background.

an expanded view of the zero-field-cooled temperature-dependent magnetization curve for $(FeRh)_5Cu_{95}$ ribbons annealed to 500 °C is shown. The paramagnetic background of the annealed $(FeRh)_5Cu_{95}$ ribbon was obtained by fitting the $M(T)$ data in the temperature range $10\,K \leq T \leq 90\,K$ to Eq. (1). From Fig. 5(b), it is clear that the temperature dependence of the magnetic moment of the annealed $(FeRh)_5Cu_{95}$ ribbons after subtraction of the paramagnetic contribution is remarkably similar to the magnetostructural phase transition trend observed in equiatomic FeRh at $T_t \sim 350$ K (antiferromagnetic-to-ferromagnetic phase transition).[15] As shown in Fig. 6(a), under an applied field of 100 Oe, a reproducible hysteresis width of ~8 K is observed in the field-cooled temperature-dependant magnetization curve of $(FeRh)_5Cu_{95}$ ribbons annealed at 500 °C. It is to be noted that thermal hysteresis is a characteristic feature of first-order magnetostructural phase transformations. Fig. 6(b) shows that the net magnetization of the $(FeRh)_5Cu_{95}$ ribbons at the transition increases upon annealing to higher temperatures, with an increased apparent Curie temperature.

At higher temperatures ($T \geq 200$ K), field-dependent magnetization measurements indicate a co-existence of paramagnetic and ferromagnetic phases. Figure 7(a) shows the development of the field-dependent magnetization behavior of the $(FeRh)_5Cu_{95}$ ribbons as a function of annealing temperature. Annealing at higher temperatures increases the saturation magnetization (M_s) of the ferromagnetic phases while decreasing the susceptibility (χ) of the paramagnetic phase, as shown in Fig. 7(b).

It is important to note that unlike the $Cu_{95}(FeRh)_5$ ribbons, the control samples—rapidly solidified $Cu_{98}Fe_2$ and $Cu_{98}Rh_2$ ribbons—did not exhibit an unexpected hysteretic magnetic transition upon thermal annealing. Akin to earlier reports in literature, the as-quenched $Cu_{98}Fe_2$ ribbons exhibited a multiphase state encompassing spin-glass ($T_b = 6.5$ K), paramagnetic and ferromagnetic phases,[35,36] while the as-quenched $Cu_{98}Rh_2$ ribbons were diamagnetic with a mass susceptibility of -7.3×10^{-7} emu/g at room temperature.[37]

IV. DISCUSSION

Nanoprecipitates of FeRh (~10 nm) were synthesized via heat treatment of a rapidly solidified phase-separated system of overall composition $Cu_{95}(FeRh)_5$. Characterization of the $Cu_{95}(FeRh)_5$ ribbons using structural and magnetic probes indicates that the properties of the FeRh nanoparticles obtained in this study differ significantly from those of bulk FeRh. In bulk form, FeRh possesses a cubic B2 (CsCl-type) crystal structure that exhibits an abrupt and hysteretic magnetic transition (AFM → FM on heating) at $T \sim 370$ K.[9] However, the FeRh nanoparticles (~10–14 nm diameter) synthesized in the present study are found to have an $L1_0$ (AuCu I type) crystal structure and exhibit a sharp, hysteretic magnetic transition at $T \sim 130$ K.

In Table I, the lattice parameter values of the $L1_0$-ordered FeRh nanoprecipitates obtained in this study are reported along with those of related intermetallic compounds, namely, $L1_0$-ordered FePt and FePd. Although the lattice parameters of the $L1_0$ FeRh nanoprecipitates are greater than those of FePd and FePt, the lattice distortion (as quantified by the c/a ratio of $L1_0$ structure) is comparable. The $L1_0$ phase of FeRh has previously been reported in near-

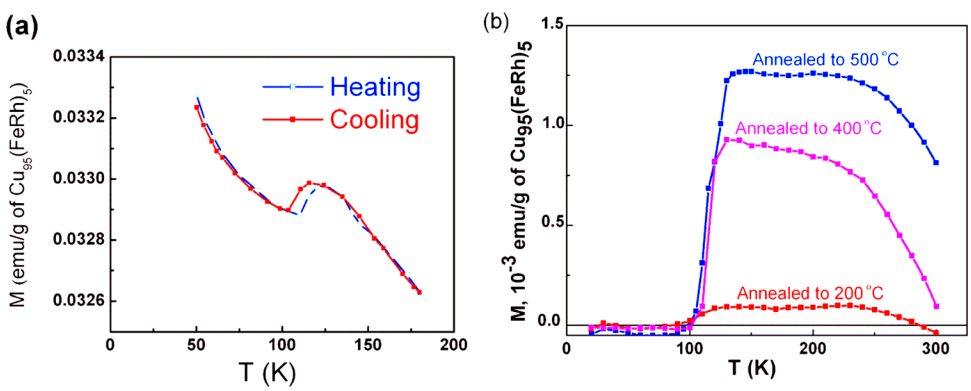

FIG. 6. (a) Thermal hysteresis in the field-cooled magnetization curve of $(FeRh)_5Cu_{95}$ ribbons annealed to 500 °C identifies a first-order-like transition that is typical of bulk FeRh. (b) Evolution of the magnetic transition at $T = 130$ K with annealing temperature reveals that while the onset of ferromagnetism at $T = 130$ K becomes more pronounced, the apparent Curie temperature T_c of the secondary phase appears to increase with increase in annealing temperature.

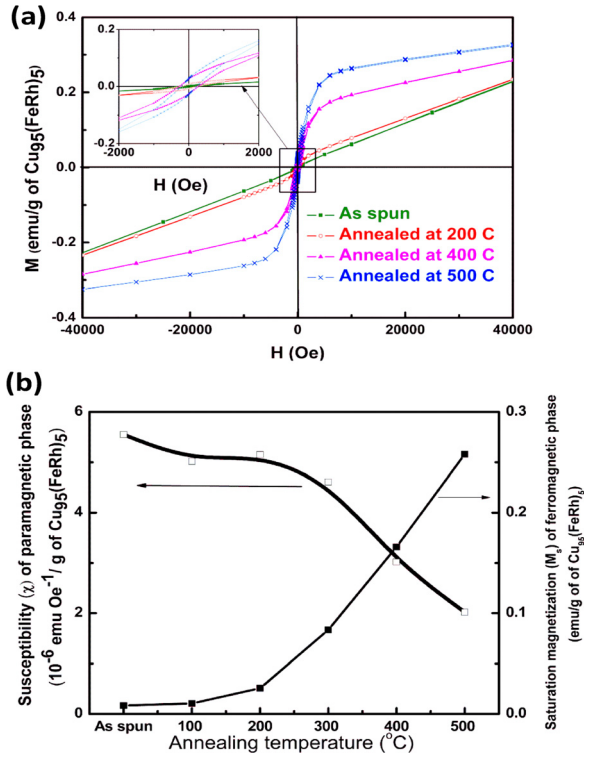

FIG. 7. Magnetic behavior of $(FeRh)_5Cu_{95}$ ribbons in the high-temperature regime ($T \geq 200$ K) indicates co-existence of paramagnetic and ferromagnetic phases. (a) Field-dependent magnetization behavior of the $(FeRh)_5Cu_{95}$ ribbons as a function of annealing temperature. (b) Annealing at higher temperatures increases the M_s of the ferromagnetic phase while decreasing the χ of the paramagnetic phase.

stoichiometric bulk FeRh alloys subjected to mild cold working[38,39] and in chemically modified bulk alloys of composition $FeRh_{1-x}M_x$ (M = Pt, Pd, x > 0.2).[20,21] As schematically depicted in Fig. 2(b), this metastable $L1_0$ phase is recognized as a stress-induced martensitic phase that may be obtained from the B2 crystal structure by twinning along the (110) plane followed by a lattice distortion along the *c*-axis.[34]

At the current time, the existence of the $L1_0$-ordered phase in the nanostructured FeRh system is tentatively attributed to combination of two effects: (a) interfacial strain derived from the coherent relationship between the FeRh precipitates and the fcc Cu matrix (Fig. 1(b)) and (b) chemical modification due to the postulated inclusion of Cu in the FeRh nanoprecipitates. It is speculated that the fcc crystal structure of the Cu matrix serves as a template for the stabilization of the $L1_0$ structure in the FeRh nanoprecipitates.

Temperature- and field-dependent magnetization studies of rapidly solidified $(FeRh)_5Cu_{95}$ ribbons indicate the existence of a complex multiphase state that includes spin-glass, ferromagnetic and paramagnetic phases. The paramagnetic and spin-glass phases in the $(FeRh)_5Cu_{95}$ ribbons are ascribed to the formation of a dilute metastable solid solution of Cu(Fe) upon rapid solidification.[35,36] The temperature-independent component of the paramagnetic phase (χ_{pp}) is largely attributed to the Cu matrix.[40] As noted from Table II, the decrease in the Curie-Weiss constant (*C*) and increase in the Pauli paramagnetic susceptibility (χ_{pp}) with increasing annealing temperature are indicative of the changing microstructure of $(FeRh)_5Cu_{95}$ ribbons upon annealing. It is proposed that annealing fosters precipitation of FeRh-based nanoparticles as suggested by the increase in saturation magnetization of the ferromagnetic phase and decrease in susceptibility of the paramagnetic phase in the $(FeRh)_5Cu_{95}$ ribbons with increased annealing time and temperature (Fig. 7). Two observations obtained via magnetic characterization of the $(FeRh)_5Cu_{95}$ ribbons strongly support the conclusion that the nanoprecipitates are indeed comprised of FeRh: (1) the remarkable similarity between the hysteretic magnetic transition at $T = 130$ K observed in annealed $(FeRh)_5Cu_{95}$ ribbons and the magnetostructural phase transition response of bulk FeRh alloys at $T \sim 350$ K (Fig. 5(b)) and (2) the conspicuous absence of a low temperature magnetic phase transition in the annealed control samples (rapidly solidified $Cu_{98}Rh_2$ and $Cu_{98}Fe_2$ ribbons).

It is reported that bulk FeRh alloys subjected to mild cold working simultaneously exhibit the $L1_0$ FeRh phase, the chemically ordered B2 FeRh phase, and the chemically disordered fcc FeRh phase.[38,39] The existence of the magnetostructural phase transition in the pure $L1_0$ FeRh phase has not, to date, been confirmed in the literature. However, a reduced first order magnetic phase transition temperature has been reported in $L1_0$-type ordered chemically modified alloys of $FeRh_{1-x}Pt_x$ alloys ($0.72 \leq x \leq 0.81$)[18] ($\Delta T_t = T_t^{Bulk\ FeRh} - T_t^{FeRh1-xPtx} \sim 200$ K). It is to be noted that the FeRh nanoparticles synthesized in this study also demonstrate a significant reduction in the magnetostructural transition temperature ($\Delta T_t = T_t^{Bulk\ FeRh} - T_t^{Nanostructured\ FeRh} \sim 220$ K).

TABLE I. Crystallographic properties of the $L1_0$ crystal structure of FeRh, FePt, and FePd.

System	Lattice parameters (Å)		Lattice distortion	Reference
	a	*c*	(*c*/*a* ratio)	
FeRh	4.32	4.20	0.97	Current study
FePt	3.85	3.71	0.96	Ref. 41
FePd	3.83	3.66	0.96	Ref. 42

TABLE II. Curie constant (C), paramagnetic Curie temperature (θ), and Pauli paramagnetic susceptibility (χ_{pp}) of the as-spun and annealed $(FeRh)_5Cu_{95}$ ribbons as obtained from fit of data to $\left(\chi_{tot} = \frac{C}{T-\theta} + \chi_{pp}\right)$.[a]

Annealing temperature (°C)	Curie constant, *C* (cm^3/g of $Cu_{95}(FeRh)_5$)	Paramagnetic Curie temperature, θ (K)	Pauli paramagnetic susceptibility, χ_{pp} (cm^3/g of $Cu_{95}(FeRh)_5$)
As-spun	1.98×10^{-3}	0.69	1.93×10^{-5}
200	1.98×10^{-3}	0.51	3.09×10^{-5}
400	1.66×10^{-3}	2.65	9.29×10^{-5}
500	4.26×10^{-4}	4.4	2.47×10^{-4}

[a]The data reported in this table were calculated by the fitting the $M(T)$ data in the temperature range $10\,K \leq T \leq 90\,K$ to Eq. (1).

V. CONCLUSIONS

The experimental evidence presented here indicates that in addition to the extrinsic variables (temperature, pressure, and magnetic field), nanostructuring may also provide a

potential route for controlling magnetostructural phase transitions in functional materials systems. Nanoprecipitates of FeRh (~10 nm) were synthesized via thermal annealing of a rapidly solidified alloy of nominal atomic composition $(FeRh)_5Cu_{95}$. These FeRh nanoprecipitates exhibit a $L1_0$ (CuAu 1)-type structure, instead of the anticipated B2 (CsCl)-type structure found in bulk FeRh. A thermally hysteretic magnetic transition, remarkably similar to the magnetostructural transition of bulk CsCl-type FeRh reported at $T_t = 370$ K, is observed in the nanostructured material at T = 130 K. This result emphasizes the sensitivity of the magnetic and structural properties of FeRh to changes in microstructural scale. To further confirm the crystal structure of the FeRh precipitates, particularly in the vicinity of the 130 K magnetic transition, and to understand the influence of interfacial strain on the magnetostructural response of the FeRh nanoprecipitates, future work aimed at advanced structural and chemical characterizations of the $(FeRh)_5Cu_{95}$ ribbons using temperature-dependant synchrotron X-ray diffraction, high-resolution transmission electron microscopy (HR-TEM), and electron energy-loss spectroscopy (EELS) is planned.

ACKNOWLEDGMENTS

Research was performed under the auspices of the U.S. Department of Energy, Division of Materials Science, Office of Basic Energy Sciences under Contract No. DE-SC0005250 [R.B., F.J.V., and L.H.L.] and the National Science Foundation, Division of Materials Research under Grant Nos. 0907007 [D.H.] and 0820521 [J.E.S.].

[1]S. B. Roy, P. Chaddah, V. K. Pecharsky, and K. A. Gschneidner, Jr., Acta Mater. **56**(20), 5895 (2008).
[2]V. D. Buchelnikov, A. N. Vasiliev, V. V. Koledov, S. V. Taskaev, V. V. Khovaylo, and V. G. Shavrov, Phys. Usp. **49**, 871 (2006).
[3]V. K. Pecharsky, K. A. Gschneidner, Jr., Y. Mudryk, and D. Paudyal, J. Magn. Magn. Mater. **321**, 3541 (2009).
[4]A. Aliev, A. Batdalov, S. Bosko, V. Buchelnikov, I. Dikshtein, V. Khovailo, V. Koledov, R. Levitin, V. Shavrov, and T. Takagi, J. Magn. Magn. Mater. **372**, 2040 (2004).
[5]D. F. Ostergaard, J. Appl. Phys. **63**, 3185 (1988).
[6]S. Otani, H. Hiraishi, M. Midorikawa, M. Teshigawara, H. Fujitani, and T. Saito, Proc. SPIE **3988**, 2 (2000).
[7]D. S. Rodbell and C. P. Bean, J. Appl. Phys. **33**, 1037 (1962).
[8]I. P. Suzdalev, Russ. J. Gen. Chem. **72**, 551 (2002).
[9]M. Fallot and R. Hocart, Rev. Sci. **8**, 498 (1939).
[10]F. de Bergevin and L. Muldawer, C. R. Acad. Sci. **252**, 1347 (1961).
[11]P. A. Algarabel, M. R. Ibarra, C. Marquina, A. del Moral, J. Galibert, M. Iqbal, and S. Askenazy, Appl. Phys. Lett. **66**, 3061 (1995).
[12]M. P. Annaorazov, S. A. Nikitin, A. L. Tyurin, K. A. Asatryan, and A. Kh. Dovletov, J. Appl. Phys. **79**, 1689 (1996).
[13]R. Z. Levitin and B. K. Ponomarev, J. Exp. Theor. Phys. (USSR) **23**, 984 (1966).
[14]R. C. Wayne, Phys. Rev. **170**, 523 (1968).
[15]D. Bloch, Ann. Phys. **1**, 93 (1966).
[16]A. I. Zakharov, A. M. Kadomtseva, R. Z. Levitin, and E. G. Ponyatovskii, J. Exp. Theor. Phys. **46**, 2003 (1964).
[17]J. S. Kouvel, J. Appl. Phys. **37**, 1257 (1966).
[18]M. Takahashi and R. Oshima, Mater. Trans., JIM **36**, 735 (1995).
[19]Paul H. L. Walter, J. Appl. Phys. **35**, 938–939 (1964).
[20]H. Miyajima, S. Yuasa, and Y. Otani, Jpn. J. Appl. Phys., Part I **32**, 232 (1993).
[21]S. Yuasa, H. Miyajima, and Y. Otani, J. Phys. Soc. Jpn. **63**, 3129 (1994).
[22]I. Suzuki, T. Koike, M. Itoh, T. Taniyama, and T. Sato, J. Appl. Phys. **105**, 07E501 (2009).
[23]S. Maat, J. U. Thiele, and E. E. Fullerton, Phys. Rev. B **72**, 214432 (2005).
[24]C. C. Chao, P. Duwez, and C. C. Tsuei, J. Appl. Phys. **42**, 4282 (1971).
[25]A. Hernando and E. Navarro, Mater. Sci. Forum **343**, 787 (2000).
[26]Z. Jia, J. W. Harrell, and R. D. K. Misra, Appl. Phys. Lett. **93**, 022504 (2008).
[27]M. A. Turchanin, P. G. Agarval, and I. Y. Nikolaenko, J. Phase Equilib. **24**, 307 (2003).
[28]D. J. Chakrabarti and D. E. Laughlin, Bull. Alloy Phase Diagr. **2**, 460 (1982).
[29]L. H. Lewis and Konrad M. Bussmann, Rev. Sci. Instrum. **67**, 3537 (1996).
[30]G. A. Nowak and A. A. Colville, Am. Miner. **74**, 488 (1989).
[31]M. E. Starumanis and L. S. Yu, Acta Cryst. A **25**, 676 (1966).
[32]C. T. Schamp and W. A. Jesser, Ultramicroscopy **103**, 165 (2005).
[33]M. Kato, M. Wada, A. Sato, and T. Mori, Acta Mater. **37**, 749 (1989).
[34]A. G. Khachaturyan, S. M. Shapiro, and S. Semenovskaya, Mater. Trans. JIM **33**, 278 (1992).
[35]K. Adachia, T. Uchiyamaa, M. Matsuia, M. Doib, and T. Miyazakib, J. Magn. Magn. Mater. **54**, 115 (1986).
[36]S. J. Campbell and T. J. Hicks, J. Phys. F: Met. Phys. **5**, 27 (1975).
[37]H. R. Khan, Ch. J. Rauba, and N. Harmsen, Mater. Res. Bull. **8**, 1131 (1973).
[38]R. Oshima, F. Hori, Y. Kibata, M. Komatsu, and M. Kiritani, Mater. Sci. Eng. A **350**, 139 (2003).
[39]M. Takahashi and R. Oshima, J. de Phys. IV **C8**, 491 (1995).
[40]F. Bitter, A. R. Kaufmann, C. Starr, and S. T. Pan, Phys. Rev. **60**, 134 (1941).
[41]T. J. Klemmer, N. Shukla, C. Liu, X. W. Wu, E. B. Svedberg, O. Mryasov, R. W. Chantrell, and D. Weller, Appl. Phys. Lett. **81**, 2220 (2002).
[42]K. Sato and Y. Hirotsu, J. Appl. Phys. **93**, 6291 (2003).